THE JOURNAL OF BIOLOGICAL CHEMISTRY Vol. 278, No. 28, Issue of July 11, pp. 26208–26215, 2003
Printed in U.S.A.

Structural Basis for Variation in Adenovirus Affinity for the Cellular Coxsackievirus and Adenovirus Receptor*

Received for publication, February 11, 2003, and in revised form, April 15, 2003
Published, JBC Papers in Press, April 25, 2003, DOI 10.1074/jbc.M301492200

Jason Howitt‡, Maria C. Bewley, Vito Graziano, John M. Flanagan, and Paul Freimuth§

From the Biology Department, Brookhaven National Laboratory, Upton, New York 11973

The majority of adenovirus serotypes can bind to the coxsackievirus and adenovirus receptor (CAR) on human cells despite only limited conservation of the amino acid residues that comprise the receptor-binding sites of these viruses. Using a fluorescence anisotropy-based assay, we determined that the recombinant knob domain of the fiber protein from adenovirus serotype (Ad) 2 binds the soluble, N-terminal domain (domain 1 (D1)) of CAR with 8-fold greater affinity than does the recombinant knob domain from Ad12. Homology modeling predicted that the increased affinity of Ad2 knob for CAR D1 could result from additional contacts within the binding interface contributed by two residues, Ser^{408} and Tyr^{477}, which are not conserved in the Ad12 knob. Consistent with this structural model, substitution of serine and tyrosine for the corresponding residues in the Ad12 knob (P417S and S489Y) increased the binding affinity by 4- and 8-fold, respectively, whereas the double mutation increased binding affinity 10-fold. X-ray structure analysis of Ad12 knob mutants P417S and S489Y indicated that both substituted residues potentially could form additional hydrogen bonds across the knob-CAR interface. Structural changes resulting from these mutations were highly localized, implying that the high tolerance for surface variation conferred by the stable knob scaffold can minimize the impact of antigenic drift on binding specificity and affinity during evolution of virus serotypes. Our results suggest that the interaction of knob domains from different adenovirus serotypes with CAR D1 can be accurately modeled using the Ad12 knob-CAR D1 crystal structure as a template.

Interaction of animal viruses with their cellular receptors is of particular interest because the viral proteins that function in molecular recognition are subject to immunoselective pressure to vary their antigenic structure. The potentially negative impact of antigenic variation on recognition of the cellular receptor is minimized in some virus families by protein structural features that shield receptor-binding sites from attack by host-neutralizing antibodies (1). In adenoviruses, by contrast, receptor-binding sites are exposed and highly variable in sequence. Therefore, adenovirus-receptor interaction presents an opportunity to observe the range of structural plasticity that can be tolerated without loss of binding specificity.

Receptor-binding function in adenoviruses is associated with viral fibers (2, 3), rod-shaped homotrimeric proteins (4) that protrude from each vertex of the icosahedral virus capsid. The distal end of viral fibers consists of a globular domain, the head or knob domain, which has receptor binding activity (5, 6). Human adenoviral fiber proteins have evolved to recognize several different host cell receptors (7–9); however, to date only one of these receptors has been molecularly characterized, a 46-kDa membrane glycoprotein known as the coxsackievirus and adenovirus receptor (CAR)[1] (10, 11). Representative serotypes from adenovirus subgroups A, C, D, E, and F have been shown to interact with CAR (12), suggesting that CAR may be the most common receptor used by human adenoviruses. The CAR protein spans the cell plasma membrane once and has two extracellular Ig domains derived from the N-terminal region of the polypeptide. The CAR N-terminal Ig variable-type domain (D1) alone is necessary and sufficient for interaction with the fiber protein knob domain (13–15). CAR has a broad tissue distribution (16) and is found predominantly on the basolateral surfaces of epithelial cells (17, 18). CAR is localized specifically within tight junctions (19, 20), which hold lateral cell membranes in close apposition to form an effective seal close to the apical surface. Although interaction of viruses with receptors such as CAR that have low expression levels on cell apical surfaces appears paradoxical, recent studies suggest that this arrangement could facilitate the spread of virus infection within tissues and transmission of virus particles to new hosts, because progeny virus particles are released preferentially from the basal-lateral surfaces of infected cells (19, 21).

X-ray structures of recombinant knob domains from the fiber proteins of adenovirus serotypes 2, 3, 5, and 12 have been determined (22–25) and in all cases show that knob monomers fold into similar 8-stranded β-sandwich conformations. Knob monomers assemble into remarkably stable trimers (26), resulting from a large number of hydrogen bonds and hydrophobic interactions in the noncovalent trimer interface (23). Variations in polypeptide chain length are accommodated by changes in the length of surface loops, whereas other sequence variations appear to have had minimal effects on the underlying β-sandwich scaffold. Structures of CAR D1 alone and in complex with the Ad12 knob also have been solved (24, 27). CAR D1 has a β-sandwich fold that is characteristic of Ig variable domains (28, 29). The x-ray structure of the Ad12 knob-CAR D1 binary complex indicates that no conformational rearrangement occurs in either molecule upon complex forma-

* This work was supported by Grant R01-AI36251 from the United States Public Health Service and by a grant from the United States Department of Energy Office of Biological and Environmental Research under Contract DE-AC02-98CH10886. The costs of publication of this article were defrayed in part by the payment of page charges. This article must therefore be hereby marked "*advertisement*" in accordance with 18 U.S.C. Section 1734 solely to indicate this fact.

‡ Present address: Dept. of Biological Sciences, Biophysics Section, Blackett Laboratory, Imperial College London, Prince Consort Road, London SW7 2BW, UK.

§ To whom correspondence should be addressed: Biology Dept., Brookhaven National Laboratory, Upton, NY 11973. Tel.: 631-344-3350; Fax: 631-344-3407; E-mail: freimuth@bnl.gov.

[1] The abbreviations used are: CAR, coxsackievirus and adenovirus receptor; D1, domain 1; Ad, adenovirus serotype; PDB, Protein Data Bank.

tion and that over 50% of the Ad12 knob-CAR D1 interfacial contacts involve residues within the knob AB loop, with the knob DE and EG loops also providing additional contact residues (24). Mutational analysis of the CAR binding activities of Ad5 and Ad12 knobs is consistent with the Ad12 knob-CAR D1 x-ray structure, suggesting that the location of the CAR D1-binding sites on knob domains from different serotypes is conserved (24, 30). The trimeric knob domain has three identical binding sites for CAR D1 that can be occupied simultaneously, as observed in the x-ray structure of the binary complex and in surface plasmon resonance experiments (24, 31).

Alignment of the Ad12 knob amino acid sequence with sequences of knob domains from other CAR-binding serotypes indicated that contact residues are not well conserved. For example, of the 15 total contact residues in Ad12 knob, only six are identical in the Ad5 knob, whereas eight are identical in the knob from Ad41L (32). This extensive variation of contact residues implies that the mechanism of knob-CAR interaction could differ significantly among adenovirus serotypes. Individual contact residues at structurally analogous positions might differ considerably in their relative contributions to binding affinity, as suggested recently in a comparison of the interaction of recombinant knob domains from Ad5 and Ad9 with CAR D1 (31, 32). One question arising from such studies is whether the relative positions of knob and CAR D1 in binary complexes changes significantly with the variation of contact residues in the knob component. This question could be addressed directly by solving crystal structures of knob-CAR binary complexes, but so far we have been unable to obtain diffracting crystals of binary complexes involving knob domains from any adenovirus serotypes other than Ad12, for reasons not presently understood. In this study, we investigated the structural basis for the difference in affinity between Ad2 and Ad12 knob for CAR D1 by first constructing homology models of Ad2 knob-CAR D1 binary complexes to predict important differences in contact residues between the two serotypes. Ad12 knob mutants were then constructed to test these predictions, both in functional binding assays and ultimately in crystal structure determination of binary complexes of the mutant knob proteins with CAR D1. Together, our results suggest that mutation of individual contact residues, as might occur during antigenic drift, in many cases only incrementally decreases affinity for the receptor. Partial retention of binding affinity may enable mutant viruses to successfully infect host cells and subsequently acquire secondary mutations that either restore high affinity binding or shift binding specificity to a novel receptor. Avidity effects resulting from the trivalent binding mechanism of knob may further compensate for mutations that weaken binding affinity, as suggested previously (31, 33, 34).

EXPERIMENTAL PROCEDURES

Protein Expression and Purification—Recombinant knob domain from Ad12 fiber protein and the N-terminal domain of CAR (CAR D1) were prepared as described previously (15). The recombinant knob domain from Ad2 fiber protein was prepared following the same protocol used for Ad12 knob. Briefly, PCR products encoding the Ad2 and Ad12 fiber knob domains and several flanking amino acids from the fiber shaft (Ad2 knob residues 387–582 and Ad12 knob residues 401–587) were cloned between the *Nde*I and *Bam*HI restriction endonuclease cleavage sites of vector pET15b (Novagen Inc., Madison, WI). The constructs were transformed into strain BL21-DE3 (Novagen Inc., Madison, WI) for expression of the hexahistidine-tagged knob proteins. All of the knob variants were constructed by primer-directed PCR mutagenesis (mutagenic primers: Ad12 knob P417S, GCAGTTTGGTGATGGGTCAGGAG; Ad12 knob S489Y, TCTATATCCCCAGTAAGCTTGAGGAA; Ad2 knob S408P, TGCAGTTAGGAGGTGGGTCTGGG; and Ad2 knob Y477S, TTCTAAAGTTCCAAGAATGTTTTTTAAGT) and cloned as above. The proteins were purified via ion exchange and nickel-nitriloacetic acid affinity chromatography (Qiagen Inc., Valencia, CA), and the molecular weight of each construct was confirmed by mass spectrometry. Each soluble expressed knob protein formed stable trimers, as assessed by nondenaturing (native) polyacrylamide gel electrophoresis and SDS-polyacrylamide gel electrophoresis of unheated protein samples. PCR products encoding CAR D1 (CAR residues 21–143, numbering from the N-terminal signal peptide) with and without the S46C mutation were cloned between the *Nco*I and *Xho*I restriction endonuclease cleavage sites of pET15b. A stop codon was omitted from the reverse primer to extend the CAR D1 C terminus with a 22-residue peptide encoded by vector sequences. This peptide extension was found to increase folding of CAR D1 in the *Escherichia coli* cytoplasm (15). CAR D1 proteins were expressed in strain BL21-DE3 and were purified by ion exchange chromatography. CAR D1 mutation S46C was constructed by primer-directed mutagenesis, using the mutagenic oligonucleotide primer GTCTTCGGGACAAAGCGTAAATTTG.

Labeling of CAR D1 S46C—Serine 46 of CAR D1 was converted to cysteine by primer-directed mutagenesis, and the resulting protein was purified by ion exchange chromatography. CAR D1 S46C protein was covalently labeled with 6-iodoacetamidefluorescein through the introduced reactive thiol group of C46. The S46C protein (2.4 mg/ml) was reduced for 90 min in buffer A (20 mM $NaPO_4$, pH 8.0, 200 mM NaCl) containing 20 mM dithiothreitol. Excess dithiothreitol then was removed on a Sephadex G-10 spin column equilibrated in buffer A. The reduced protein was collected directly into a receiving tube containing 1.5 times molar excess of 6-iodoacetamide fluorescein, and the mixture was incubated for 4 h at 25 °C in the dark with end-over-end tumbling. Excess 6-iodoacetamide fluorescein was removed by gel filtration on a Sephedex G-10 column (60 × 15 mm) in buffer A. The degree of labeling was determined spectrophotometrically by measuring the absorbance of the labeled protein at 280 and 492 nm. Wild type CAR D1 control protein remained unlabeled after treatment by this procedure, indicating that only the introduced cysteine group of the S46C mutant was reactive.

Fluorescence Anisotropy Experiments—Equilibrium binding experiments were performed on a Tecan Ultra 384 plate reader (Tecan, Salzburg, Austria) using flat bottomed, black, 96-well, untreated microplates (Nalge Nunc Int., Naperville, IL). The reaction mixtures contained 5 nM of fluorescein-labeled CAR D1 S46C in binding buffer (10 mM Tris-HCl, pH 8.0, 0.1 mM EDTA, 0.0125% Nonidet P-40) with varying concentrations of knob proteins (10 nM to 5 μM). The total reaction volume was 300 μl, and the plates were incubated at 25 °C for 30 min. The fluorometer was set up with excitation and emission wavelength filters of 485 and 535 nm, respectively, and with a fluorescein dichroic mirror. The integration time was 40 μs, with 10 lamp flashes/measurement. The gain and optimal Z-position were determined manually using a control prior to the start of the experiment. The anisotropy values were calculated as the ratio of the difference between vertical and horizontal emission intensities ($I_{//}$ and $I_{\perp}$) normalized to the total intensity (Equation 1). Factor G is the ratio of the sensitivities of the detection system for vertically and horizontally polarized light.

$$A = (I_{//} - GI_{\perp}) / (I_{//} + 2GI_{\perp}) \qquad \text{(Eq. 1)}$$

The equilibrium binding curves were analyzed using Table Curve (SPSS Inc., Chicago, IL). Binding curves obtained for the knob-CAR interaction were fitted to an A + B → AB model that describes single-site independent binding of ligand to the receptor. This model assumes that complexes form with no multivalent avidity effects, because both the receptor and the ligand are free in solution during the analysis.

Competitive displacement studies were performed by titrating 5 nM of labeled CAR D1 S46C to ~90% saturation with 650 nM knob domain from Ad2 fiber protein and then back titrating the complexes with unlabeled wild type CAR D1 while measuring the decrease in fluorescence anisotropy. The results of the concentration-dependent decrease in anisotropy were fitted according to the equations of Huff *et al.* (35). Because the concentration of CAR D1 in the anisotropy assays (5 nM) was well below the reported dissociation constant for CAR D1 homodimers (16 μM) (27), the protein can be regarded as monomeric under the conditions used.

Modeling—Homology modeling of Ad2 knob in complex with CAR D1 was performed using Swiss PDB Viewer (36). The Ad12 knob-CAR D1 binary complex was used as a template (PDB code 1KAC), and Ad2 knob was superimposed on the structure, 1.04 Å root mean square deviation for α-carbon atoms. Visual inspection of this model indicated potential contacts at the interface of Ad2 knob and CAR D1 that are not observed in the Ad12 knob-CAR D1 structure. The residues at the complex interface that were not conserved between Ad2 and Ad12 knob were modeled in the context of Ad12 knob in all rotomer conformations.

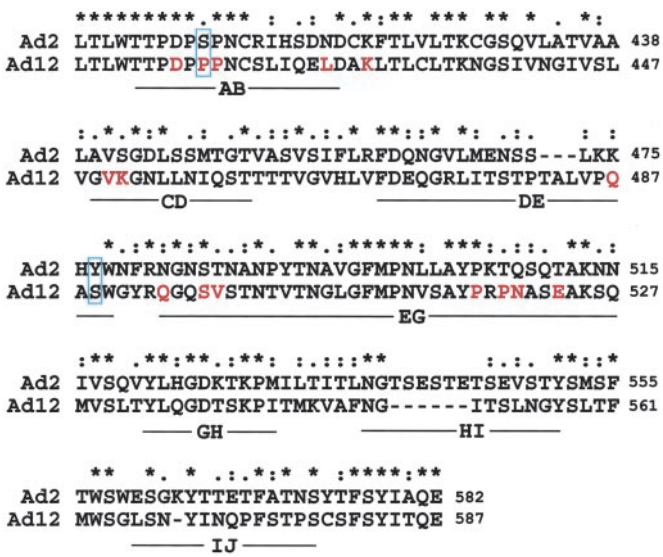

FIG. 1. **Sequence alignment of Ad2 and Ad12 knob.** Sequences of Ad2 knob residues 399–582 and Ad12 knob residues 408–587 were aligned using ClustalX (42). Conserved residues are indicated with a *asterisk*, and similar residues are indicated with *one* or *two dots*. Loop regions are *underlined* and named. Highlighted in *red* are residues of Ad12 knob that contact CAR D1 in the Ad12 knob-CAR D1 crystal structure. Residues mutated in this study are *boxed* in *blue*. Six of the 15 Ad12 knob residues involved in contacts with CAR D1 are strictly conserved in Ad2 knob. Of the remaining nine Ad12 knob contact residues, seven correspond to conservative substitutions (indicated by *dots*), and two correspond to nonconservative substitutions in Ad2 knob.

Positive and negative potential interactions were scored using the Swiss PDB Viewer mutation tool.

Crystallization—Crystals of purified knob-CAR D1 complexes were grown at room temperature by the sitting drop vapor diffusion method. All of the reagents used were obtained from Hampton Research (Hampton Research, Laguna Niguel, CA). Protein drops contained 2 μl of protein solution and 2 μl of reservoir solution, and the wells contained 500 μl of crystallization buffer. Crystals of Ad12 knob P417S-CAR D1 were grown in 3.2 M ammonium sulfate in 100 mM HEPES, pH 7.0. The crystals of the Ad12 knob S489Y-CAR D1 were grown in 0.8 M ammonium sulfate in 100 mM HEPES, pH 7.0. The crystals were flash cooled at 99 K with 50% ethylene glycol as a cryoprotectant.

Data Collection and Model Refinement—In each case, full data sets were collected from single crystals using a 4 cell CCD on National Synchrotron Light Source Beamline X25 at Brookhaven National Laboratory (Upton, NY). The data were processed using the HKL Program suite (37) as summarized in Table II. The protein coordinates of 1KAC were subjected to rigid body refinement in CNS after a 5 Å region around the mutant site had been omitted. A cycle of torsion angle refinement at 5000 K was performed prior to initial $F_o - F_c$ and $2F_o - F_c$ electron density map calculation. The electron density for the substituted amino acids could be assigned unambiguously. The final refinement statistics are shown in Table II. The coordinates for the P417S-CAR D1 and S489Y-CAR D1 structures were deposited in the PDB and assigned PDB codes 1P69 and 1P6A, respectively.

RESULTS

Fluorescence Anisotropy Assay and Design of Knob Variants—The residues involved in the recognition of CAR D1 are not strictly conserved within the knob domains of fiber proteins from different adenovirus serotypes (Fig. 1). To assess the effects of this variation on binding affinity, we developed a fluorescence anisotropy-based assay that measures interaction of knob and CAR D1 in solution. This assay limits multivalent avidity effects that can arise when either knob or CAR D1 is immobilized on a two-dimensional surface, because it measures the affinity of individual binding sites on the trivalent knob molecule. For this assay, a reactive sulfhydryl group was introduced into CAR D1 to permit site-specific labeling with fluorescein. Serine 46 was chosen for conversion to cysteine based on its surface exposure and its location outside of the knob-binding surface of CAR D1 (Fig. 2*C*). Spectroscopic analysis showed that the CAR D1 S46C mutant protein was quantitatively labeled after reaction with 6-iodoacetamide fluorescein, whereas no incorporation of fluorescein was detected in control reactions containing wild type CAR D1 protein (data not shown). Formation of knob-CAR D1 complexes was monitored by the increase in fluorescence anisotropy upon incubation of fluorescein-labeled CAR D1 S46C with increasing, subsaturating concentrations of knob protein (Fig. 2*A*). To determine whether the fluorescein label influenced the interaction of CAR D1 with the knob proteins, a competitive displacement experiment was performed. Fluorescein-labeled CAR D1 S46C was titrated to ~90% saturation with Ad2 knob protein, and the complexes were then back titrated with wild type unlabeled CAR D1 (Fig. 2*B*). The data were fitted to a displacement curve to determine the inhibition constant (K_i). The dissociation constant (K_d) of the forward titration and the K_i of the back titration were equivalent to within 3% error, indicating that the labeled CAR D1 S46C protein retained binding activity similar to that of wild type CAR D1.

Using this anisotropy assay, we measured the binding affinities of two different serotypes of adenovirus knob, Ad2 and Ad12, toward CAR D1. Equilibrium binding affinities were derived from binding isotherms, as reported in Table I. Ad2 knob bound to CAR D1 with a K_d of 35 nM, whereas Ad12 knob bound to CAR D1 with a K_d of 295 nM. To investigate the basis for this 8-fold difference in affinity, we constructed a homology model (rigid body interaction) of the Ad2 knob-CAR D1 complex (Fig. 3). Because the main chain conformations of Ad2 and Ad12 knob are similar (α-carbon atoms have root mean square deviation of 1.04 E), Ad2 knob was built into the homology model in the same relative orientation as that of Ad12 knob in the crystallographically determined Ad12 knob-CAR D1 complex. No steric clashes were observed at the binding interface, suggesting that the homology model reasonably approximated the actual structure of the Ad2 knob-CAR D1 complex.

Six contact residues of Ad12 knob are strictly conserved in Ad2 knob, and all of these appear to contact CAR D1 in the homology model of Ad2 knob-CAR D1. Seven contact residues of Ad12 knob are conservatively substituted in Ad2 knob, and three of these Ad2 knob residues (Asn^{482}, Thr^{486}, and Thr^{507}) appear to contact CAR D1, whereas three others (Ser^{442}, Lys^{475}, and Gln^{508}) are more distant from CAR D1 and thus may contribute less to binding affinity. The final Ad2 knob residue in this group, Ser^{408}, appeared to form an additional hydrogen bond with CAR D1 that is not observed in the Ad12 knob-CAR D1 complex. The remaining two contact residues of Ad12 knob (Leu^{426} and Glu^{523}) correspond to nonconservative substitutions in Ad2 knob. Ad12 knob residue Leu^{426} forms a main chain hydrogen bond with CAR D1, and the corresponding Ad2 knob residue, Asn^{417}, also is within hydrogen bonding distance from CAR D1 in the homology model. Ad12 knob Glu^{523} forms hydrophobic contacts with CAR D1, but the corresponding Ad2 knob residue (Thr^{511}) is too distant from CAR D1 to make similar contacts. However, small rearrangements of the EG loop compared with its position in the model potentially could enable Thr^{511} to contact CAR D1. In summary, homology modeling suggested that 4 of the 15 residues of Ad2 knob that correspond to contact residues in Ad12 knob may not be oriented favorably to contact CAR D1. Consequently, we searched the homology model further for additional potential contact residues that could account for the greater affinity of Ad2 knob for CAR D1.

It was observed that one Ad2 knob residue in particular,

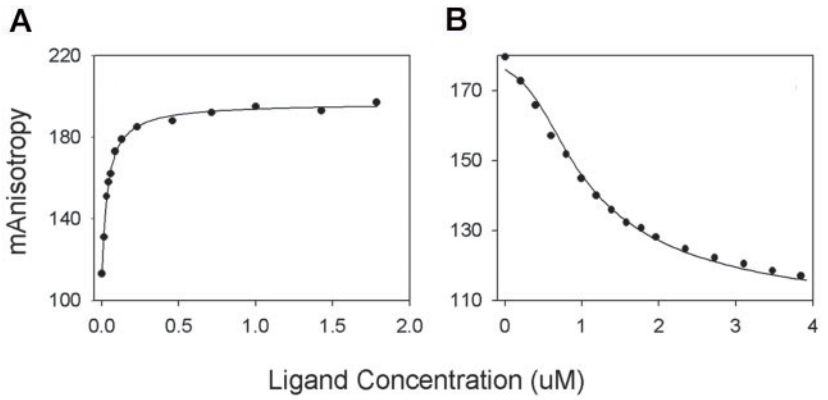

FIG. 2. **Analysis of knob-CAR D1 interactions using equilibrium fluorescence anisotropy.** *A*, equilibrium binding curve of Ad2 knob with labeled CAR D1 S46C. *B*, displacement of labeled CARD1 S46C from Ad2 knob by wild type CAR D1. Labeled CAR D1 S46C was back titrated from a near saturating concentration of Ad2 knob using an increasing amount of wild type CAR D1. *C*, stereo view of CAR D1 mutant S46C in ribbon representation. The side chain of residue 46 is highlighted in *yellow*. Residues that interact directly with Ad12 knob are shown in ball and stick representation.

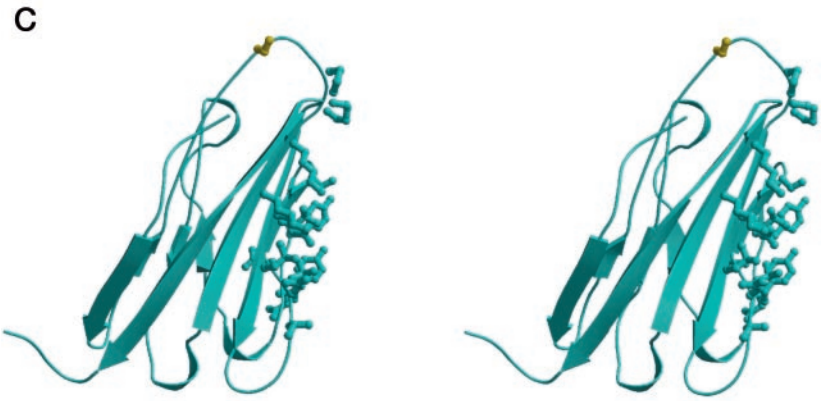

TABLE I
Equilibrium binding affinities of adenovirus knob domains for CAR D1 obtained through fluorescence anisotropy measurements
The results are the means ± S.D. of triplicate measurements.

Adenovirus knob	K_d
	nM
Ad2 wild type	35 ± 1.8
Ad2 S408P	85 ± 1.8
Ad2 Y477S	3600 ± 23
Ad12 wild type	290 ± 48
Ad12 P417S	76 ± 4.1
Ad12 S489Y	35 ± 4.4
Ad12 P417S-S489Y	28 ± 4.4

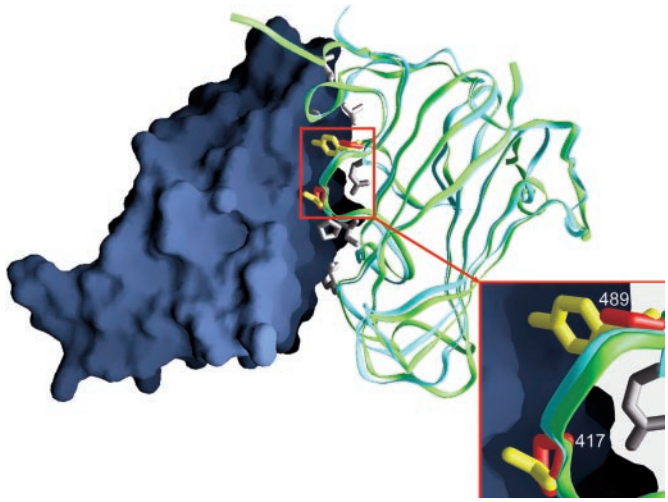

FIG. 3. **Homology model of Ad2 knob bound to CAR D1.** The x-ray structure of Ad2 knob was overlaid onto Ad12 knob in the x-ray structure of the Ad12 knob-CAR D1 complex. For simplicity, only one monomer of the knob trimer is shown. The surface of CAR D1 (space-filling model on *left*) is colored *blue*. Superimposed ribbon structures of Ad2 knob and Ad12 knob are colored *cyan* and *green*, respectively. Side chain residues of Ad12 knob contacting CAR D1 are shown in *gray* except for side chains of Ser^{489} and Pro^{417}, which are shown in *red*. Ad2 knob Ser^{408} and Tyr^{477} side chains are colored *yellow*.

Tyr^{477}, was within hydrogen bonding distance of CAR D1 and that its side chain was able to make additional contacts at the complex interface. Tyr^{477} is positioned within a region that forms a cavity in the Ad12 knob-CAR D1 complex (Fig. 3). Modeling of tyrosine at the corresponding position in Ad12 knob, Ser^{489}, indicated that a tyrosine residue at this position could be accommodated in the Ad12 knob-CAR D1 interface and could form two additional hydrogen bonds with CAR D1. Therefore, the overall results of homology modeling suggested that the increased affinity of Ad2 knob for CAR D1 could result from additional contacts contributed by Ad2 knob residues Ser^{408} and Tyr^{477}.

To test the importance of Ser^{408} and Tyr^{477} in the interaction of Ad2 knob with CAR D1, these residues were mutated to the corresponding residues in Ad12 knob, proline and serine, respectively, and the interaction of the resulting Ad2 knob mutants S408P and Y447S with CAR D1 was characterized in the fluorescence anisotropy assay (Fig. 4). The affinity of Ad2 knob S408P was decreased by approximately a factor of 2, whereas the affinity of Ad2 knob Y477S was decreased ~100-fold (Table I). The converse mutants also were constructed to determine whether additional contacts contributed by these residues would increase the binding affinity of Ad12 knob. Equilibrium binding studies showed that the resulting Ad12 knob mutants P417S and S489Y both had increased affinity for CAR D1 (Table I and Fig. 4), consistent with the model that the side chains of both mutant residues make positive contacts with CAR D1. A double mutant, introducing both point mutations into Ad12 knob, further increased the binding affinity to 28 nM,

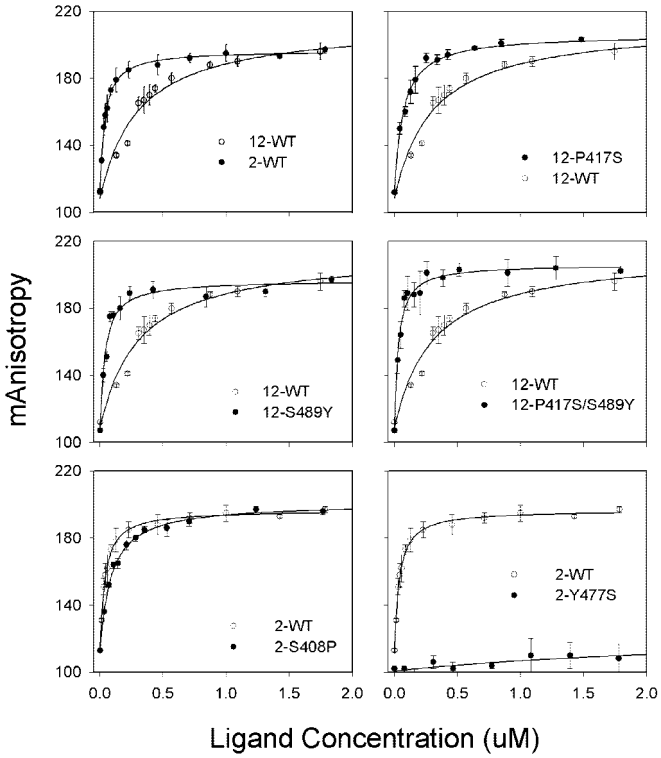

FIG. 4. **Anisotropy measurements of fluorescein-labeled S46C-CAR D1 with adenovirus knob variants.** The results are the means of triplicate measurements. The *error bars* represent the standard deviations. *WT*, wild type.

greater than the observed affinity of wild type Ad2 knob for CAR D1 (Fig. 4).

X-ray Structures of Ad12 Knob Mutants in a Binary Complex with CAR D1—To further investigate the interactions that contribute to the increased binding affinity of the Ad12 knob mutants P417S and S489Y, x-ray structures of the two mutant proteins in binary complexes with CAR D1 were solved to ~3 Å resolution (Table II). Data sets were essentially isomorphous to the native data sets, resulting in corresponding structures that are very similar to the native structure. Backbone atoms of wild type Ad12 knob-CAR D1 and Ad12 knob P417S-CAR D1 were superimposable with a root mean square deviation of 0.1 Å, indicating that the overall main chain structures are identical and that CAR D1 was bound in the same conformation and orientation in both the mutant and wild type complexes. Backbone atoms of wild type Ad12 knob-CAR D1 and Ad12 knob S489Y-CAR D1 also were superimposable with a root mean square deviation of 0.1 Å, again indicating identical conformations and orientation of bound CAR D1. The β-hydroxyl group of the serine residue introduced into the AB loop of Ad12 knob (P417S) is within hydrogen bonding distance of the Oϵ1 atom of CAR D1 residue Glu^{56} (Fig. 5*b*) and thus potentially could form an additional hydrogen bond within the knob-CAR D1 interface. No other conformational changes, with the exception of a rotation of the side chain of CAR D1 residue Asp^{54} at the Cβ atom, were observed compared with the structure of the wild type binary complex, suggesting that the increase in affinity of this mutant may be a direct consequence of the serine residue at position 417. The crystal structure of the Ad12 knob S489Y-CAR D1 complex indicated that the extended length of the tyrosine residue side chain at residue 489 increased its potential to form additional hydrogen bonds with CAR D1 that cannot form by the corresponding serine residue in wild type Ad12 knob. The −OH group of knob residue Tyr^{489} was within hydrogen bonding distance of the backbone oxygen and nitrogen atoms of CAR D1 residues Pro^{52} and Ala^{125} (Fig. 6*b*). Rotation of the side chain of CAR D1 residue Asp^{54} again was the only observed change in conformation as compared with the wild type Ad12 knob-CAR D1 structure. The substantial increase in affinity of Ad12 knob mutant S489Y for CAR D1 therefore likely results from formation of two additional hydrogen bonds and burial of the tyrosine aromatic side chain.

DISCUSSION

Evolution of adenoviruses under immunoselective pressure has resulted in antigenic drift of surface residues, including those within the receptor-binding sites of the fiber protein knob domain. Despite this high degree of surface variation, many adenovirus serotypes attach to cells through interaction with CAR, a membrane glycoprotein that also serves as a cellular receptor for group B coxsackieviruses. Investigation of the interaction of fiber proteins from different adenovirus serotypes with CAR D1 therefore presents an opportunity to estimate the range of solutions to the molecular recognition problem that occur in a natural system. With the exception of Ad12 knob, it has so far not been possible to directly view the interaction of knobs from other adenovirus serotypes with CAR by x-ray crystallography. Here we circumvented this problem by using the x-ray structure of Ad12 knob-CAR D1 binary complex as a template to model contact residues on the surface of other knob serotypes and predict how binding affinity and specificity might be affected by variation of contact residues.

Ad2 knob was chosen for this initial modeling study because it binds to CAR D1 with significantly greater affinity than does Ad12 knob (Table I). Equilibrium binding studies were performed using fluorescence anisotropy measurements of CAR D1 labeled with fluorescein at a specific site. Affinity values calculated from the anisotropy measurements were lower (weaker) than have been previously observed in other *in vitro* assays, such as surface plasmon resonance (31, 32). These differences in affinity probably can be attributed to the absence of avidity effects in complex formation. In binding assays such as surface plasmon resonance, either the receptor or the ligand is immobilized, thereby limiting the association event to a two-dimensional surface. By contrast in the fluorescence anisotropy assay used here, both interacting species are in solution, and the affinity values therefore reflect individual binding events. Although the absolute affinity values obtained by fluorescence anisotropy probably underestimate the actual overall affinity of knob for membrane-associated CAR, the values obtained by this method are useful for characterizing the contribution of individual amino acid residues within the knob-CAR interface. Equilibrium binding affinity measurements using the fluorescence anisotropy assay showed that Ad2 knob bound CAR D1 with an 8-fold greater affinity compared with Ad12 knob (Table I). The increased affinity of Ad2 knob indicates that its receptor-binding sites overall make more favorable contacts with CAR D1 than do the binding sites of Ad12 knob. Binding site fitness could be improved either by increasing the number of favorable contacts or by eliminating contacts that interfere with stable binding.

The homology model of the Ad2 knob-CAR D1 complex predicted that two residues of Ad2 knob, Ser^{408} and Tyr^{477}, could contribute additional hydrogen bonds and other contacts that may account for the greater affinity of Ad2 knob for CAR D1 (Fig. 3). These predictions were well supported by mutagenesis studies, where substitution of serine and tyrosine for the corresponding residues in Ad12 knob increased its affinity for CAR D1, whereas the converse mutations decreased the affinity of Ad2 knob for CAR D1. Prior studies using kinetic-based measurements indicated that Ad12 knob has a slower on-rate but similar off-rate compared with Ad2 and Ad5 knobs (31, 32).

TABLE II
Summary of data collection statistics

	Ad12 knob P417S-CAR D1	Ad12 knob S489Y-CAR D1
Crystal parameters		
Space group	$P4_332$	$P4_332$
Cell dimensions (Å)	a = 168.62	a = 168.93
Mathew's coefficient	5.75	5.78
No. of molecules in AU	1 knob monomer, 1 CAR D1	1 knob monomer, 1 CAR D1
Data collection		
Resolution (Å)	30–3.3	20–2.9
Unique observations	12250	18322
Redundancy	6.5	6.2
R_{merge} (%)[a]	10.6 (26.5)	8.2 (39.5)
Completeness (%)	95.4 (94.3)	97.7 (98.0)
$I/\sigma I$	11 (4)	14 (4)
Refinement statistics		
Resolution limits (Å)	25–3.3	30–2.9
No. of protein atoms	2359	2366
R factor (%)[b]	21.6	21.8
R_{free}	25.6	25.2
No. of reflections in free set	1220	869
Geometric parameters		
Bond length (Å)	0.014	0.011
Bond angle (°)	1.7	1.4

[a] $R_{merge} = \| I_{obs} \| - \| I_{avg} \| I \| I_{avg} \|$.
[b] $R = {}_{h} \| F_P \| - \| F_M \| I \| F_P \|$, where $| F_P |$ is the structure factor observed data and $| F_M |$ is the structure factor of the model. The n = numbers in parentheses refer to data in the outermost resolution shell. AU, asymmetric unit. I, intensity.

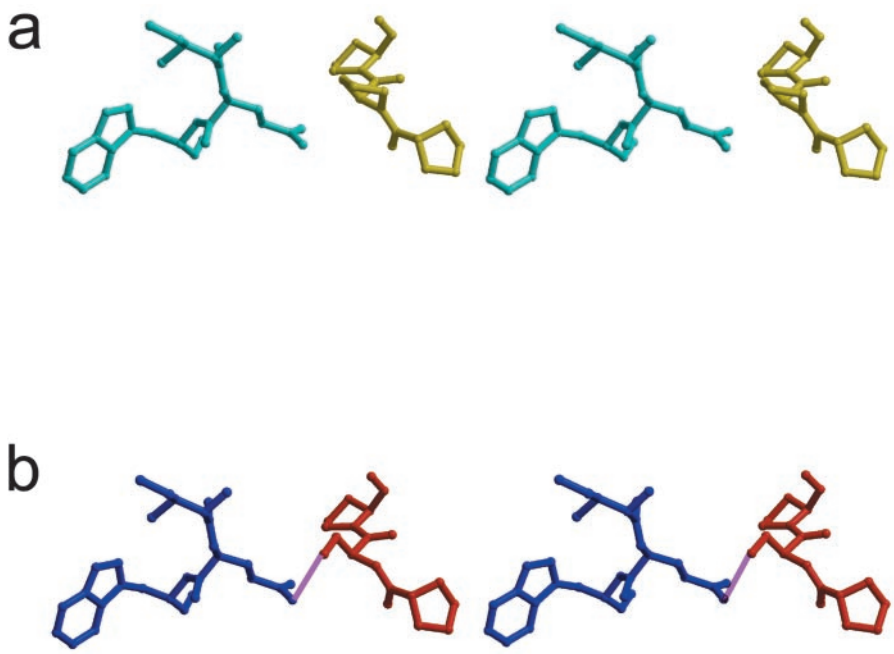

FIG. 5. **Comparison of crystal structures of wild type Ad12 knob-CAR D1 and Ad12 knob P417S-CAR D1.** *a*, stereo figure showing part of the wild type Ad12 knob-CAR D1 interface including CAR D1 residues I55-E56-W57 (*cyan*) and Ad12 knob residues P416-P417-P418 (*yellow*); no hydrogen bonds are formed at this interface. *b*, stereo figure of same view of the interface between Ad12 knob mutant P417S (*blue*) and CAR D1 (*red*); note the novel hydrogen bond formed between Ser^{417} of knob and Glu^{56} of CAR D1.

Although kinetic parameters cannot be determined from the equilibrium binding assay used here, it is likely that the P417S and S489Y mutations increase the association rate of Ad12 knob through the formation of more favorable interfacial contacts. The P417S and S489Y mutations are located in the Ad12 knob AB and DE loops, respectively, which is consistent with the earlier conclusion that individual residues within these two loops make substantial contributions to binding affinity (24, 30). Importantly, whereas several earlier studies have predicted contact residues in knob serotypes based on amino acid sequence alignments with Ad12 knob (14, 24, 30, 32, 38), here through the use of homology modeling we were able to identify a novel contact residue in Ad2 knob (Y477) that does not have a functionally equivalent counterpart in Ad12 knob. Substitution of tyrosine for the positionally equivalent residue in Ad12 (Ser^{489}) resulted in an 8-fold increase in binding affinity.

To directly investigate the contribution of individual residues to binding affinity, we crystallized and solved the structures of two Ad12 knob mutants, P417S and S489Y, in complex with CAR D1. No changes in the relative positions of knob and CAR D1 components were detected in the resulting 3 Å resolution structures, as compared with the wild type complex, and no significant perturbations of the Ad12 knob structure were detected for either mutant. The structures support predictions from modeling studies that each substituted residue forms additional hydrogen bonds with CAR D1. Homology modeling also predicted that the protruding aromatic side chain of Ad2 knob residue Tyr^{477} would reduce the size of a cavity that forms in the Ad12 knob-CAR D1 interface (24), possibly excluding some nonstructural water molecules that become trapped in the Ad12 knob-CAR D1 complex. Burial of an aromatic side chain can play a critical role in stabilizing protein-protein interactions. For example, in the interaction of human immunodeficiency virus with its cellular receptor CD4, insertion of CD4 residue F43 into a cavity on the surface of gp120 accounts for 23% of interatomic contacts at the interface (39). The 100-

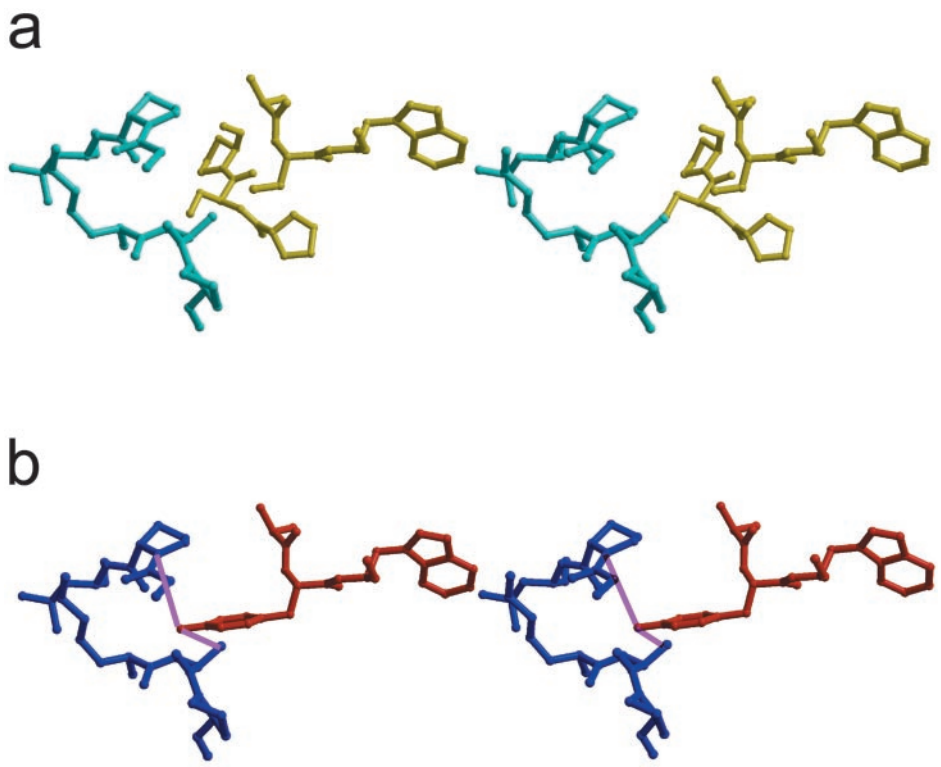

FIG. 6. **Comparison of crystal structures of wild type Ad12 knob-CAR D1 and Ad12 knob S489Y-CAR D1.** *a*, stereo figure showing part of the wild type Ad12 knob-CAR D1 interface including CAR D1 residues Gly^{51}-Pro^{52}-Leu^{53} and Lys^{124}-Ala^{125}-Pro^{126} (*cyan*) and Ad12 knob residues Ala^{488}-Ser^{489}-Trp^{490} (*yellow*); no atoms are within hydrogen bonding distance at this interface. *b*, same view of the interface between Ad12 knob mutant S489Y (*blue*) and CAR D1 (*red*). Note that Tyr^{489} of knob makes two novel hydrogen bonds with Pro^{52} and Ala^{125} of CAR D1.

fold decrease in Ad2 knob binding affinity resulting from mutation Y477S indicates that Tyr^{477} also makes a large contribution to binding affinity, although the precise role of the residue cannot be fully understood without determining a high resolution structure of the Ad2 knob-CAR D1 complex. The relatively smaller effect of tyrosine at the equivalent position in Ad12 knob (mutant S489Y) suggests that the contribution of individual contact residues to binding affinity may be context-dependent. At 3 Å resolution it was not possible to determine the impact of the S489Y mutation on the size and solvent content of interfacial cavities.

The high degree of variation in contact residues among CAR-binding serotypes and the observed tight range of binding affinities (variations over a ~10-fold range have been measured by surface plasmon resonance (31, 32) with the exception of Ad9 knob (32)) suggest that the knob domain architecture may be specialized to minimize the impact of mutations on binding site structure and function. The receptor binding sites of knob consist of surface loops that are supported by an unusually stable, trimeric scaffold, and in this regard have a similar architecture to the antigen binding sites of antibodies. Although the range of molecular targets recognized by knob domains of natural adenoviruses appears limited to a small number of cellular receptors, this narrow range undoubtedly reflects the strong selective pressure on the virus to retain sufficient binding affinity to successfully infect host cells. It is probable that the natural evolution of binding specificity is a multi-step process where the loss of affinity for the initial receptor and gain of affinity for a novel receptor occur simultaneously. Multivalent binding may compensate for relatively weak or low affinity binding at individual sites, enabling virus to bind tightly enough to infect host cells (31). In addition, certain adenovirus serotypes have two independent fiber genes (40), which may have provided an alternate means for independent evolution of novel binding specificity. Changes in fiber protein binding specificity during virus evolution likely contributed to the overall success of adenoviruses as human and animal pathogens. The utility of adenovirus-based vectors for use in gene therapy or as recombinant virus vaccines also might be enhanced by rational modification of fiber protein binding specificity. The availability of bacterial expression systems for recombinant knob domain (5) and of methods for structure-guided mutagenesis and directed protein evolution (41) now can be exploited to investigate the potential of the knob scaffold to interact with a broad range of molecular targets.

Acknowledgment—We thank Karen Springer for excellent technical assistance.

REFERENCES

1. Rossmann, M. G. (1989) *J. Biol. Chem.* **264,** 14587–14590
2. Philipson, L., Lonberg-Holm, K., and Pettersson, U. (1968) *J. Virol.* **2,** 1064–1075
3. Levine, A. J., and Ginsberg, H. S. (1967) *J. Virol.* **1,** 747–757
4. van Oostrum, J., and Burnett, R. M. (1985) *J. Virol.* **56,** 439–448
5. Henry, L. J., Xia, D., Wilke, M. E., Deisenhofer, J., and Gerard, R. D. (1994) *J. Virol.* **68,** 5239–5246
6. Louis, N., Fender, P., Barge, A., Kitts, P., and Chroboczek, J. (1994) *J. Virol.* **68,** 4104–4106
7. Wu, E., Fernandez, J., Fleck, S. K., Von Seggern, D. J., Huang, S., and Nemerow, G. R. (2001) *Virology* **279,** 78–89
8. Stevenson, S. C., Rollence, M., White, B., Weaver, L., and McClelland, A. (1995) *J. Virol.* **69,** 2850–2857
9. Defer, C., Belin, M. T., Caillet-Boudin, M. L., and Boulanger, P. (1990) *J. Virol.* **64,** 3661–3673
10. Tomko, R. P., Xu, R., and Philipson, L. (1997) *Proc. Natl. Acad. Sci. U. S. A.* **94,** 3352–3356
11. Bergelson, J. M., Cunningham, J. A., Droguett, G., Kurt-Jones, E. A., Krithivas, A., Hong, J. S., Horwitz, M. S., Crowell, R. L., and Finberg, R. W. (1997) *Science* **275,** 1320–1323
12. Roelvink, P. W., Lizonova, A., Lee, J. G., Li, Y., Bergelson, J. M., Finberg, R. W., Brough, D. E., Kovesdi, I., and Wickham, T. J. (1998) *J. Virol.* **72,** 7909–7915
13. Wang, X., and Bergelson, J. M. (1999) *J. Virol.* **73,** 2559–2562
14. Kirby, I., Davison, E., Beavil, A. J., Soh, C. P., Wickham, T. J., Roelvink, P. W., Kovesdi, I., Sutton, B. J., and Santis, G. (2000) *J. Virol.* **74,** 2804–2813
15. Freimuth, P., Springer, K., Berard, C., Hainfeld, J., Bewley, M., and Flanagan, J. (1999) *J. Virol.* **73,** 1392–1398

16. Bergelson, J. M., Krithivas, A., Celi, L., Droguett, G., Horwitz, M. S., Wickham, T., Crowell, R. L., and Finberg, R. W. (1998) *J. Virol.* **72,** 415–419
17. Walters, R. W., Grunst, T., Bergelson, J. M., Finberg, R. W., Welsh, M. J., and Zabner, J. (1999) *J. Biol. Chem.* **274,** 10219–10226
18. Zabner, J., Freimuth, P., Puga, A., Fabrega, A., and Welsh, M. J. (1997) *J. Clin. Invest.* **100,** 1144–1149
19. Walters, R., Freimuth, P., Moninger, T., Ganske, I., Zabner, J., and Welsh, M. (2002) *Cell* **110,** 789–799
20. Cohen, C. J., Shieh, J. T., Pickles, R. J., Okegawa, T., Hsieh, J. T., and Bergelson, J. M. (2001) *Proc. Natl. Acad. Sci. U. S. A.* **98,** 15191–15196
21. Spear, P. G. (2002) *Dev. Cell* **3,** 462–464
22. Xia, D., Henry, L. J., Gerard, R. D., and Deisenhofer, J. (1994) *Structure* **2,** 1259–1270
23. van Raaij, M. J., Louis, N., Chroboczek, J., and Cusack, S. (1999) *Virology* **262,** 333–343
24. Bewley, M. C., Springer, K., Zhang, Y. B., Freimuth, P., and Flanagan, J. M. (1999) *Science* **286,** 1579–1583
25. Durmort, C., Stehlin, C., Schoehn, G., Mitraki, A., Drouet, E., Cusack, S., and Burmeister, W. P. (2001) *Virology* **285,** 302–312
26. Hong, J. S., and Engler, J. A. (1996) *J. Virol.* **70,** 7071–7078
27. van Raaij, M. J., Chouin, E., van der Zandt, H., Bergelson, J. M., and Cusack, S. (2000) *Struct. Fold. Des.* **8,** 1147–1155
28. Harpaz, Y., and Chothia, C. (1994) *J. Mol. Biol.* **238,** 528–539
29. Williams, A. F., and Barclay, A. N. (1988) *Annu. Rev. Immunol.* **6,** 381–405
30. Roelvink, P. W., Mi Lee, G., Einfeld, D. A., Kovesdi, I., and Wickham, T. J. (1999) *Science* **286,** 1568–1571
31. Lortat-Jacob, H., Chouin, E., Cusack, S., and van Raaij, M. J. (2001) *J. Biol. Chem.* **276,** 9009–9015
32. Kirby, I., Lord, R., Davison, E., Wickham, T. J., Roelvink, P. W., Kovesdi, I., Sutton, B. J., and Santis, G. (2001) *J. Virol.* **75,** 7210–7214
33. Baranowski, E., Ruiz-Jarabo, C. M., and Domingo, E. (2001) *Science* **292,** 1102–1105
34. Wang, J. (2002) *Trends Biochem. Sci.* **27,** 122–126
35. Huff, S., Matsuka, Y. V., McGavin, M. J., and Ingham, K. C. (1994) *J. Biol. Chem.* **269,** 15563–15570
36. Guex, N., and Peitsch, M. C. (1997) *Electrophoresis* **18,** 2714–2723
37. Otwinowski, Z., and Minor, W. (1997) *Methods Enzymol.* **276,** 307–326
38. Kirby, I., Davison, E., Beavil, A. J., Soh, C. P., Wickham, T. J., Roelvink, P. W., Kovesdi, I., Sutton, B. J., and Santis, G. (1999) *J. Virol.* **73,** 9508–9514
39. Kwong, P. D., Wyatt, R., Robinson, J., Sweet, R. W., Sodroski, J., and Hendrickson, W. A. (1998) *Nature* **393,** 648–659
40. Yeh, H. Y., Pieniazek, N., Pieniazek, D., Gelderblom, H., and Luftig, R. B. (1994) *Virus Res.* **33,** 179–198
41. Patten, P. A., Howard, R. J., and Stemmer, W. P. (1997) *Curr. Opin. Biotechnol.* **8,** 724–733
42. Thompson, J. D., Gibson, T. J., Plewniak, F., Jeanmougin, F., and Higgins, D. G. (1997) *Nucleic Acids Res.* **25,** 4876–4882